Global J. Environ. Sci. Manage. 8(4): 485-502, Autumn 2022, Serial #32

Global Journal of Environmental Science and Management
(GJESM)

Homepage: https://www.gjesm.net/

ORIGINAL RESEARCH ARTICLE

Inkjet printing of metal oxide coatings for enhanced photovoltaic soiling environmental applications

E. Fares[1,2], B. Aïssa[3], R.J. Isaifan[1,*]

[1] *Division of Sustainable Development, College of Science and Engineering, Hamad Bin Khalifa University, Qatar Foundation, P.O. Box 5825, Doha, Qatar*

[2] *Department of Mechanical and Industrial Engineering, College of Engineering, Qatar University, P.O. Box 2713, Doha, Qatar*

[3] *Qatar Environment and Energy Research Institute, Hamad Bin Khalifa University, Qatar Foundation, P.O. Box 5825, Doha, Qatar*

ARTICLE INFO

Article History:
Received 23 November 2021
Revised 01 February 2022
Accepted 5 March 2022

Keywords:
Anti-soiling
Inkjet printing
Metal oxides
Nanoparticles
Photovoltaic (PV)
Solar panels
Thin films

DOI: 10.22034/gjesm.2022.04.03

ABSTRACT

BACKGROUND AND OBJECTIVES: Global energy needs have gradually shifted toward photovoltaic solar energy, especially in the Gulf region because of the high solar-irradiance potential. However, one of the main challenges for this technology in the region is soiling, which has been reported to degrade the power output of photovoltaic modules significantly. Anti-soiling coatings are promising technologies to minimize the effect of dust on photovoltaic solar panels. Accordingly, this study aimed to synthesize aluminum, zinc, titanium, and tin oxides using mixed-based and nanoparticle-based precursors through inkjet printing techniques and investigate their potential in anti-soiling applications for PV panels.

METHODS: Four metal oxides, namely, aluminum, zinc, titanium, and tin oxides, were synthesized and deposited using the inkjet printing technique for anti-soiling application. Ultraviolet-visible spectroscopy, field emission scanning electron microscope, X-ray diffraction, X-ray photoelectron spectroscopy, and contact angle measurements were performed to characterize these thin films.

FINDINGS: The optical transmittance of the substrate using the nanoparticle ink revealed better optical properties than that using the mixed-based ink. Compared with nanoparticle samples, a homogeneous crack and a defect-free layer were observed with dense nanoparticles in all mixed inks (except for aluminum oxide ink). The contact angles indicated that the synthesized films were super-hydrophilic/hydrophilic coatings. The results of the outdoor testing revealed that up to 60% less dust was deposited on the best-performing film (aluminum oxide mixed-based ink) compared with bare glass.

CONCLUSION: The outdoor experiment revealed that mixed-based thin films were better in reducing dust deposition than nanoparticle-based thin films and bare glass. This enhancement might be due to the decreased antireflection property along with a morphological contribution related to the presence of nanoparticle voids, which reduce the spectra scattering and minimize its deterioration, thus demonstrating better anti-soiling properties. The results of the outdoor test revealed that aluminum, zinc, and titanium oxides are promising materials for anti-soiling coating applications for both ink types. However, tin oxide coatings are not recommended for anti-soiling applications, as they showed the highest dust deposition rate near the bare glass performance.

NUMBER OF REFERENCES	NUMBER OF FIGURES	NUMBER OF TABLES
54	10	0

*Corresponding Author:
Email: *risaifan@hbku.edu.qa*
Phone: +974 554 7449
ORCID: 0000-0002-9590-4939

Note: Discussion period for this manuscript open until January 1, 2023 on GJESM website at the "Show Article".

INTRODUCTION

Soiling is one of the main issues inherent to photovoltaic (PV) deployment, especially in the arid region, accounting for 70 percent (%) of PV-power losses (Micheli *et al.,* 2017). Anti-soiling coating (ASC) is one of the promising mitigation techniques for dust accumulation on PV panels (Pescheux *et al.,* 2020; Lee *et al.,* 2022; Thongsuwan *et al.,* 2022), as it efficiently reduced the operational and maintenance costs and the associated cleaning water consumption, especially in the desert environment (Alnaser *et al.,* 2018; Eihorn *et al.,* 2019). The ASC concept mainly relies on hydrophobic (contact angle (CA)>90°) or hydrophilic (CA<90°) properties, which can be achieved by a surface chemistry treatment, a surface morphology modification, and/or a combination of both (Bukhari *et al.,* 2019). Few studies have addressed both parameters; however, many researchers demonstrated the utilization of silicon and titanium dioxides (SiO_2 and TiO_2) for ASC applications (Jesus *et al.,* 2018). Jesus *et al.,* (2018) used titanium and silicon dioxides (TiO_2/SiO_2), pure TiO_2, and SiO_2 thin films and experimentally tested them for 4–5 months in Italy, Spain, and Brazil. They found that the light transmittance (T%) loss of the uncoated glass was 16%, whereas the coated ones reduced the T% loss by 50%, specifically in the TiO_2/SiO_2 sample. They emphasized the importance of ASCs for dry regions. Sueto *et al.,* (2013) found that coating a photocatalytic surface layer with a modified tungsten trioxide (WO_3) and partially hydrolyzed tetraethyl orthosilicate potentially reduced the dust adhesion from 0.25 electronvolt (eV) to 0.10 eV. Moreover, accumulated sand masses were reduced from >0.01 g to 0.005 g. Furthermore, Ota *et al.,* (2016) found that silica-based coating increased the transmittance and energy output of PV panels by >3%. Bahattab *et al.,* (2016) also observed an approximately 7% increase in the transmittance when low-iron soda-lime float glass was coated with SiO_2 nanoparticles (NP). Pendse *et al.,* (2018) found that the CA was more than 130° when depositing magnesium fluoride (MgF_2) NP on glass; accordingly, light transmittance increased by 7%–9%. On the contrary, Said *et al.,* (2015) tested the difference between textured antireflective coated and uncoated PV panels. They found that the clean PV module power output increased by an average of 4%–8% when coated panels were used because of the decreased reflection losses, whereas dust fouling was mitigated by 5% with the use of textured antireflective coatings. Li *et al.,* (2013) prepared a hydrophobic antireflective SiO_2-based coating for PV panels and found that the performance was enhanced by approximately 6.6% with a maximum transmittance of 98.3%; thus, it could also be used for self-cleaning application. Likewise, Arabatzis *et al.,* (2018) reported an increase of 5%–6% in the power gain for TiO_2/SiO_2-coated PV panels compared with the uncoated ones because of the increased light transmittance in the visible region and enhanced self-cleaning. Oh *et al.,* (2016) used SiO_2 NP-based ASC. In their study, energy soiling losses reduced up to 3.85%, and the module's power improved by approximately 2.56% because of the antireflection function. Hossain *et al.,* (2021), tested silica thin films and found that PV efficiency was improved up to 27%. Similarly, Piliougine *et al.,* (2013) found a 0.8% difference in daily energy soiling losses between coated (with metal oxide NP and a hybrid polymer binder) and uncoated PV panels. All these previous studies have utilized dip-coating, spin-coating, and vapor-deposition techniques. Essentially, none of the aforementioned studies have utilized inkjet printing. However, limitations such as coating degradation, light transmittance loss, and instability for such coatings have been reported (Eihorn *et al.,* 2019; Pescheux *et al.,* 2020). For example, Pescheux *et al.,* (2020) revealed that they have subjected their coatings to accelerated aging tests to verify their durability to real outdoor exposures. However, the coatings recorded small losses of optical performances despite the aggressiveness of the tests. Nowadays, metal oxide materials are heavily used in solar cells as transparent electrodes, light absorbers, transport layers, and other functionalities such as ASC and antireflective surfaces (Perez-Tomas *et al.,* 2018). Their widespread use was attributed to their availability in nature, nontoxicity (Nunes *et al.,* 2019), low cost (Isaifan *et al.,* 2017), and fabrication processes (Perez-Tomas *et al.,* 2018). Further, they proved to be suitable for outdoor applications because of their insolubility and chemical and thermal stability (Isaifan *et al.,* 2017; Perez-Tomas *et al.,* 2018; Nunes *et al.,* 2019). Perez-Tomas *et al.,* (2018) provided evidence that mesoporous zirconia, for instance, has high stability, can be fully printed, and eliminates the use of precious metals, which are replaced by low cost carbon-based materials. Other

important properties of metal oxide materials are their large bandgap and low reflective index, which help in harvesting more photons (Perez-Tomas *et al.,* 2018; Nunes *et al.,* 2019). Based on the above reasons, metal oxides improve the device's characteristics and increase its reliability (Perez-Tomas *et al.,* 2018). Therefore, the present study focused on metal oxides for the preparation of ASC layers. TiO_2, aluminum oxide (Al_2O_3), tin oxide (SnO_2), and zinc oxides (ZnO) were used as candidates for such purposes. Inkjet printing is a valuable technique in nanotechnology, especially for metal oxide thin film fabrication (Liu *et al.,* 2015). Metal oxide precursors could be prepared using the colloidal suspension of metal oxide NP, metal salt solution, and colloidal NPs based on sol–gel chemistry. Furthermore, Liu *et al.,* (2015) recommended using colloidal NP based on sol–gel chemistry and/or metal salt solutions, as NP tended to agglomerate in the colloidal suspension of metal oxide NP. Inkjet printing has several advantages. To name a few, it has a direct patterning (Wang *et al.,* 2014), programmed printing with precise droplet volume (Liu *et al.,* 2015), low operating cost, fast production rate, and lower environmental effect than other techniques, especially vacuum-based ones (Wang *et al.,* 2014). Moreover, it is implemented in ambient temperature (Wang *et al.,* 2014) and provides quick mass production, as Liu *et al.,* (2015) stated. Metal oxide materials synthesized using inkjet printing have been widely used for different applications, such as solar cells, electronic devices, and sensors. More than 200 scientific publications have been published on this subject area during the last decade (Liu *et al.,* 2015); however, inkjet printing techniques have not been utilized yet in ASC applications. Since the size of dust particles in Qatar ranges from 0.6 micrometers (µm) to 50 µm (Javed *et al.,* 2017; Ilse *et al.,* 2018), coatings and texturing should be in nanoscale range to decrease the adhesion forces by minimizing the contact area between the dust particles and the surface (Polizos *et al.,* 2018b), and to avoid the accumulation of dust particles in between the surface voids and textures. Likewise, surface texturing size should be smaller than the solar radiation wavelength to minimize photon scattering (Polizos *et al.,* 2018b). Finally, material preparation (i.e., precursor concentration) depends highly on the employed technique. For example, to get an acceptable super hydrophobic coating, the concentration in a spray technique should be lower than the concentration if a spin-coating is used (Polizos *et al.,* 2018a) because the higher concentration of the binder masks or overcoats the silica NP and interferes with their functionality. The present study aimed to synthesize metal oxide coatings of TiO_2, Al_2O_3, SnO_2, and ZnO using mixed-based (NP and metal oxide salts) and NP-based precursors via inkjet printing techniques and investigate their potential in ASC applications for PV panels. To the best of the authors' knowledge, no study in the literature has addressed the preparation and comparison of the four metal oxide-based coatings for ASC applications prepared with the aid of inkjet material printing. Inkjet printing is easy to use and can be implemented at ambient temperature. It has several advantages over other common techniques for film fabrication, such as material efficiency and less wastage due to programmed printing with precise droplet volume, low operating cost, fast production rate, and lower environmental effect. This study was conducted in Qatar during 2021 and 2022.

MATERIALS AND METHODS

Substrate cleaning

The soda-lime glass samples (Sigma–Aldrich, MA, USA) of size 1" × 1" were used as the substrate material for the coatings. The glass substrates were cleaned to improve the ink's wettability. Substrate cleaning was performed following the procedure reported by Buffiere *et al.,* (2020).

Ink preparation

Metal nitrate hydrate based on zinc and aluminum nitrates (i.e., $Zn(NO_3)_2{\cdot}6H_2O$ and $Al(NO_3)_3 \cdot 9H_2O$), tin chloride hydrate ($SnCl_2 \cdot 2H_2O$), nanopowder (ZnO, Al_2O_3, TiO_2 nanopowder), and SnO_2 NP ink of 7–20 nanometer (nm) in size were purchased from Sigma–Aldrich. In this study, two metal oxide precursors, i.e., pure NP-based ink and mixed-based ink (salt and NP), were synthesized and deposited on the glass surface by the inkjet printing technique following the same procedure reported by Buffiere *et al.,* (2020). NP-based ink was prepared by dispersing the nanopowder with a size of 27–43 for Al_2O_3 and <100 nm for ZnO and TiO_2 in isopropanol (IPA) with a volume ratio of 25:75 (powder: IPA). Ethylene glycol (EG) was then added with a ratio of 25:75

(precursor:EG) to adjust the precursor viscosity (Rieu *et al.,* 2016), except for SnO_2 NP-based ink, a ready-made (as purchased) ink, where no further modifications have been made. EG was added to maintain the viscosity and the surface tension within an acceptable range to the inkjet printer as described previously (Cummins *et al.,* 2012). According to Liu *et al.,* (2015), the recommended viscosity for an inkjet printer was between 1 and 20 millipascal second (mPa.s) and the surface tension was between 25 and 50 millinewton per meter (mN/m) (Cummins *et al.,* 2012). Furthermore, Quan *et al.,* (2017) used a mixture of salt-based ink solutions and NP. Salt was used to lower the surface energy, and the NP was used to increase the surface roughness, which enhances the anti-soiling properties. To this end, the mixed-based precursors using both NP- and salt-based inks were prepared with equal volume for each NP and salt (1:1). The NP-based ink was prepared following the above-mentioned procedure, whereas the salt-based ink was synthesized following the protocol adopted in this paper (Rieu *et al.,* 2016). However, TiO_2 salt-based ink was prepared using a diluted solution of titanium diisopropoxide bis(acetylacetonate) (TAA) in IPA with a volume ratio of 1:20 of TAA:IPA, and a homogeneous layer was observed (Buffiere *et al.,* 2020). Fig. 1a and b show the different inks used in the present study, their synthesis process, and thin film formation mechanism.

Before printing, the ink viscosity was measured to ensure that it fits within the acceptable range (Liu *et al.,* 2015). The viscosity at 26.5 degrees Celsius (°C) for SnO_2 ink was 8.84 mPa.s, and those for Al_2O_3 and ZnO inks were 12.8 mPa.s and 11.7 mPa.s, respectively. The viscosity of TiO_2 ink was 2.3–2.6 mPa.s at 20°C. The viscosity of all inks was within the recommended range of drop-on-demand ink properties, which should be between 1 and 20 mPa.s (Liu *et al.,* 2015). After testing the ink's properties, it was loaded in the cartridge and then clipped inside the Inkjet Dimatix Materials Printer (DMP). A cartridge of 1–10 picoliter (pL) nozzle with 16 total nozzles was used. A computer connected to the printer controlled the coordinates, path, time, and number of deposition cycles.

Coating approach

In this study, Fujifilm Dimatix Materials Printer (DMP-2850) was used to deposit the metal oxide precursors. To optimize the droplet dispatching out of the cartridge, the voltage for all precursors was kept between 8 Volts (V) minimum (for the one pL nozzle cartridge) to 17 V maximum (for the 10 pL nozzle cartridge). The droplet interspacing was 30 µm, and the plate and cartridge temperature was 45°C. The 1-pL cartridge nozzle was used for all precursors, except for Al_2O_3, where 10 pL was used, as a more homogeneous layer was observed. Ten layers were deposited. After each layer, the sample was dried in the furnace at approximately 200°C for 10 minutes (min) in the air. The effects of different surface textures were investigated using different metal precursors to determine the optimal anti-soiling texture to be deposited on the glass substrate. Thus, different ink types were used in which a pure NP and a combination of metal oxide salts and NP were utilized to prepare the precursors, as shown in Fig. 1a.

Thermal annealing

To ensure that the metal oxide thin film has been formed, it was heated up to 450°C for 30 min (thermal annealing) as per the procedure performed by Buffiere *et al.,* (2020). Thermal annealing was performed at 450°C for 30 min at a heating rate of 30°C–45°C/min.

Analysis techniques

To characterize the ink properties, viscosity was measured using a Discovery Hybrid rheometer. Approximately 5 milliliters (mL) of the ink was dispensed on a standard Peltier plate, and shear was applied using 60 millimeters (mm), 1° cone geometry. The thin films were characterized concerning the optical, structural, chemical, and anti-soiling properties. Field emission scanning electron microscopy (SEM) was used to characterize the top-view morphology and topography of the coated surfaces with 5 kilovolts (kV) using a JEOL 7610F SEM system. Optical performance was assessed using an ultraviolet-visible (UV-VIS) 5000 spectrophotometer measuring direct transmittance and reflectance in the wavelength range from 248 to 1000 nm (Karabay *et al.,* 2012). The water CA was measured by an optical CA system (DSA25 Drop Shape Analyzer) with a droplet volume of 2 microliters (µL) to test the surface hydrophobicity/hydrophilicity. The water droplet was held for approximately 40 seconds (s) before photos were captured. Surface chemistry was

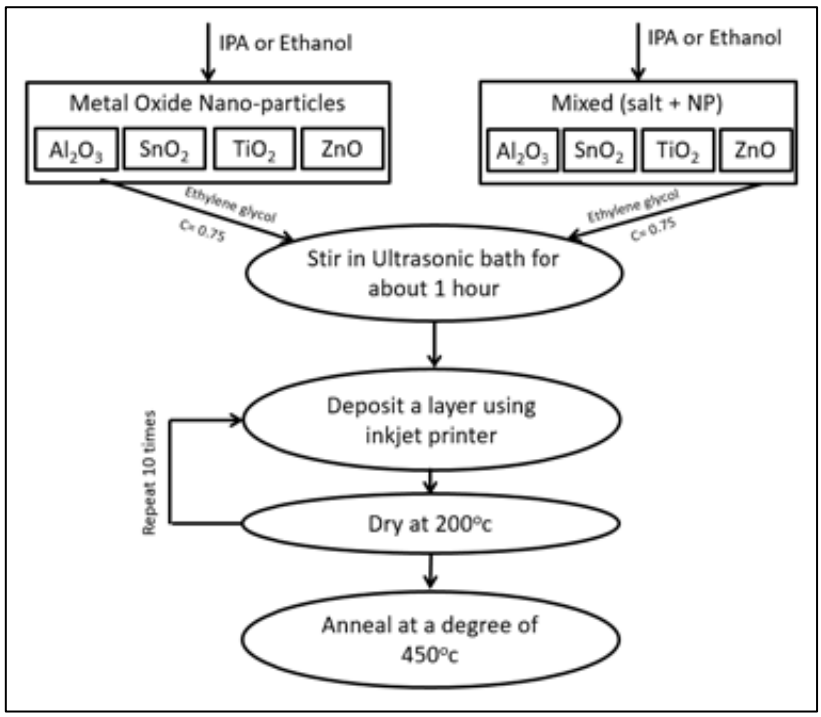

(a)

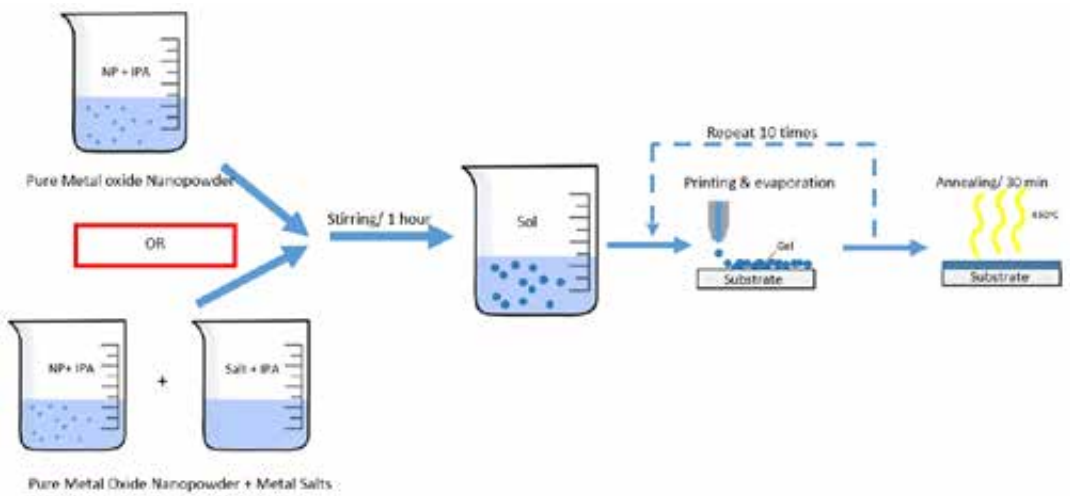

(b)

Fig. 1: Research methodology (a) Chart flow of the formation mechanism of a metal oxide thin film and (b) synthesis process based on sol–gel chemistry.

monitored using an X-ray photoelectron spectrometer (XPS; Thermo Scientific ESCALab 250Xi). X-ray powder diffraction (XRD) was performed to evaluate the crystallinity of the layer using grazing incidence XRD geometry (Rigaku SmartLab XRD), with an incidence angle of 0.2°. The X-ray generator was set at 40 kV and 30 milliamperes (mA). The measurements were performed at (2θ). The outdoor experiment was

implemented by exposing the samples to real-world environmental conditions for accurate simulation of the anti-soiling properties. The samples were located in one of the outdoor sites of the Mechanical and Industrial Engineering Department in Qatar University. They were placed at a tilt angle of 0° (facing the sky). The required climate and weather information was extracted from two weather websites: Weather Underground and Civil Aviation Authority in Qatar. During the experiment, dust removal was carefully avoided, except for natural causes, such as wind and rain. The mass of all samples was measured and recorded by a balance scale with an accuracy of 0.0001 gram (g) before the outdoor experiment. The experiment started on March 1, 2021, and lasted for 22 days. The mass of the samples was then measured regularly (every 3 days). The difference between the initial mass (before exposure) and the sample mass at each reading was recorded. Similar to the work by Isaifan *et al.,* (2017), the dust deposition rate of each sample was calculated by dividing the difference in weight by the surface area of the glass (Eq. 1).

$$Deposition\ rate = \frac{\text{Substrate mass after exposure - Substrate mass before exposure}}{\text{Substrate's surface area}} \quad (1)$$

RESULTS AND DISCUSSIONS

Optical properties

The optical transmittance (T%) and absorbance (A%) spectra in the 248–1000 nm region are shown in Fig. 2a and b for different NP and mixed thin films, respectively. In all thin film types, the performance of Al_2O_3 thin film was superior in terms of the average transmittance and reflection, followed by ZnO, TiO_2, and finally SnO_2. An average transmittance gain of 0.10% and a reflection reduction of approximately 0.08% were observed with Al_2O_3 NP thin film over the bare glass. This result agrees with those of similar studies, i.e., the transmittance of the Al_2O_3-coated substrate has increased (Kareem *et al.,* 2011). The improved performance was attributed to the reduction in reflection compared with the bare glass (Kareem *et al.,* 2011). Moreover, the NP-coated materials have better transmittance and lower reflection than the mixed thin films by approximately 0.89% and 1.21%, respectively. This might be due to nano-voids and surface roughness, which enhance the transmittance and reduce the reflection (Kauppinen *et al.,* 2017). A study reported that nanoscale texturing smaller than the solar radiation wavelength minimizes photon scattering (Polizos *et al.,* 2018b). Hence, both mixed and pure NP-coated materials have lower absorbance values than bare glass. Furthermore, the average transmittance of NP and mixed thin films was higher than 90% in the visible region, except for SnO_2 where it was higher than 85%. These results were in conformance with several studies that have reported the same observations using similar metal oxide materials (Yamaguchi *et al.,* 2005; Kareem *et al.,* 2011). Interestingly, the transmittance of TiO_2 mixed thin film in the visible region was approximately 87%, which was lower than the transmittance observed for TiO_2 of NP thin film (Arabatzis *et al.,* 2016). The absorbance A% was deduced using Eq. 2.

$$A\% = 100 - (T\% + R\%) \quad (2)$$

Structural properties

The XRD spectra of the metal oxide films were obtained after the annealing process to determine the phase and crystallographic structure (Fig. 3). The XRD data revealed that the films deposited by both precursor types (i.e., pure NP ink and mixed ink) were not crystallized, as the diffraction peaks were weak and broad. This is in agreement with previous results on the characterization of metal oxide materials (Legrand-Buscema *et al.,* 2002; Sobczyk-Guzenda *et al.,* 2013), where the phase was amorphous for films under heat treatments performed in 450°C–500°C (Legrand-Buscema *et al.,* 2002). Thus, the coated thin films were amorphous, except for the SnO_2 films. The results of the analysis of these spectra indicated that the coatings prepared from both precursor solutions correspond to the compound SnO_2 with peaks of 26°, 33°, and 52° belonging to (110), (101), and (211) planes, respectively (Aziz *et al.,* 2013). These peaks confirmed that the films were polycrystalline. The influence of the precursor type on the crystallographic orientation of the SnO_2 films was also investigated. Accordingly, the XRD patterns showed improved peak intensities of the mixed precursors compared with those of the pure NP ones. More specifically, the peak corresponding to the (110) plane indicated a preferential growth, as a higher intensity was observed over this plane. Therefore, the crystallographic characteristics

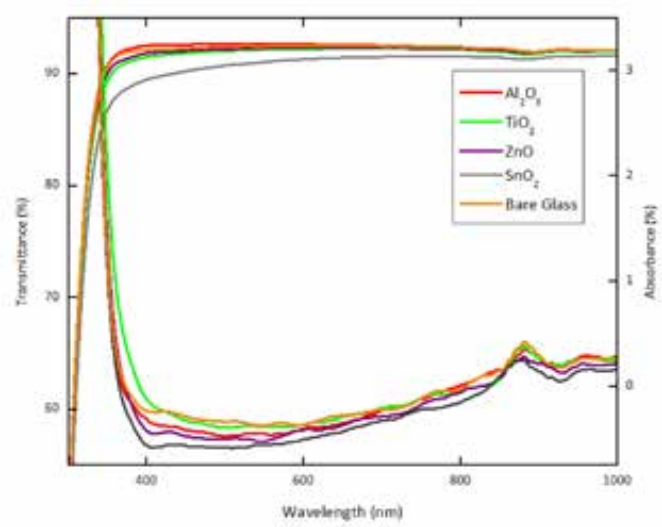

(a)

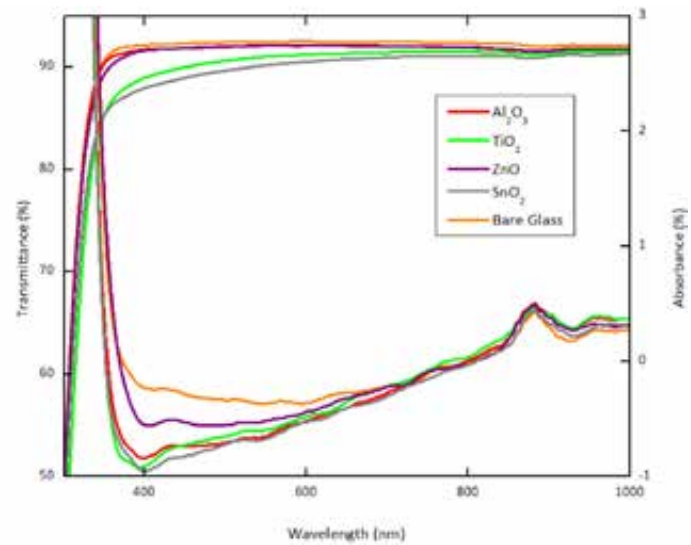

(b)

Fig. 2: Transmittance (T%) and absorbance (A%) of (a) NP films and (b) mixed films.

changed based on the precursor type, in which mixed precursors showed better crystallinity. However, the very broad peak observed around 2θ=25° in the XRD pattern of Al_2O_3 originated from the glass substrate (Huang *et al.,* 2006).

Furthermore, SEM results revealed that the coatings prepared using pure NP precursor exhibited relatively smoother and finer nano- and microstructure features in all the metal oxide samples (Fig. 4 to 7 a-c). They were uniformly distributed across the substrate area compared with the coatings prepared using mixed precursors (Fig. 4 to 7 d-f). Furthermore, the NP were more visible in the mixed precursor samples than in the pure NP precursor

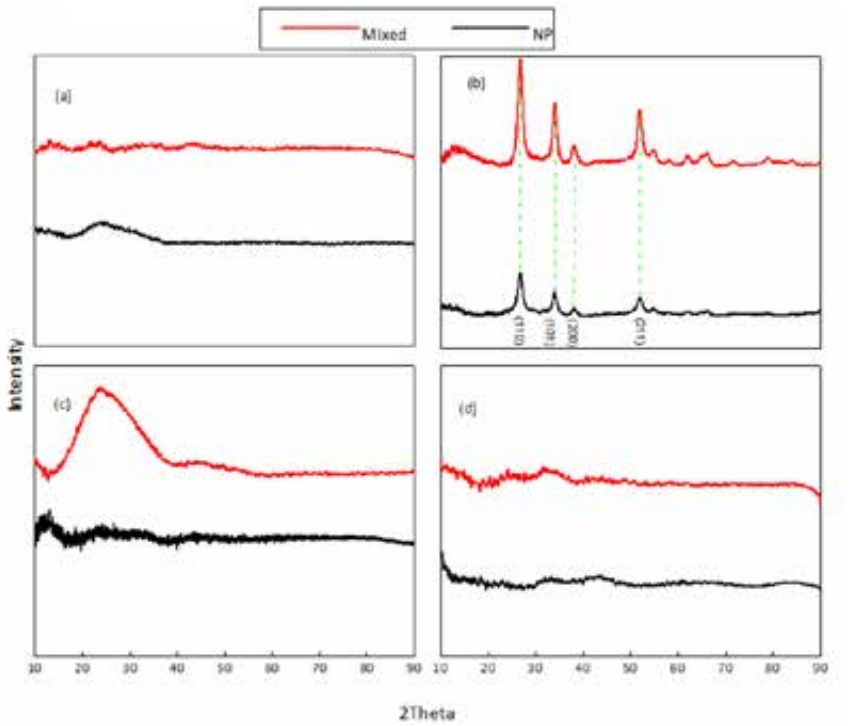

Fig. 3: XRD results for mixed and NP-based inks: (a) ZnO, (b) SnO_2, (c) Al_2O_3, and (d) TiO_2.

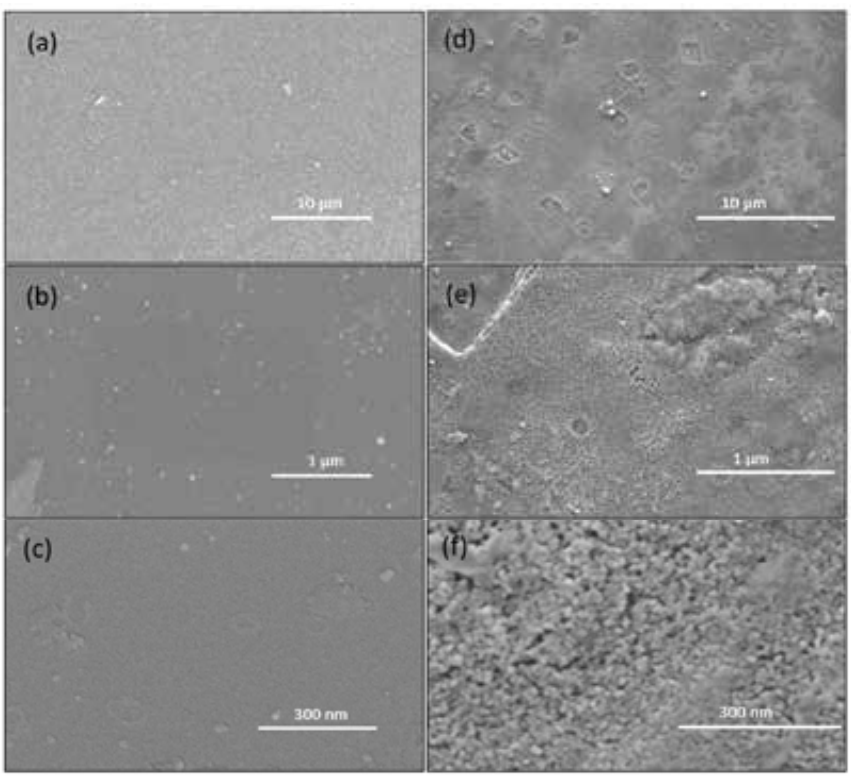

Fig. 4: SEM images for ZnO for NP-based ink (a–c), and mixed precursors NP (d–f).

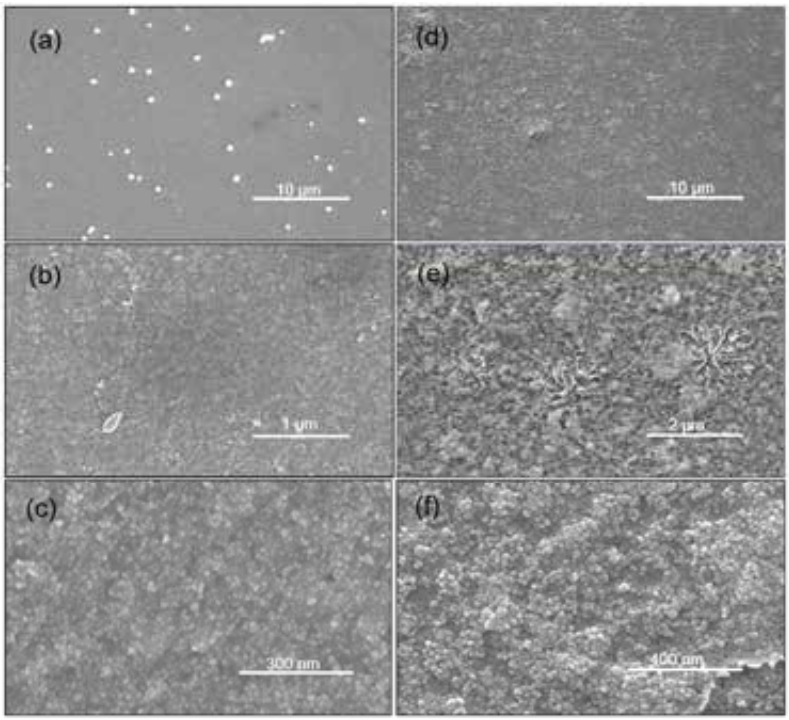

Fig. 5: SEM images for SnO_2 for NP-based ink (a–c), and mixed precursors NP (d–f).

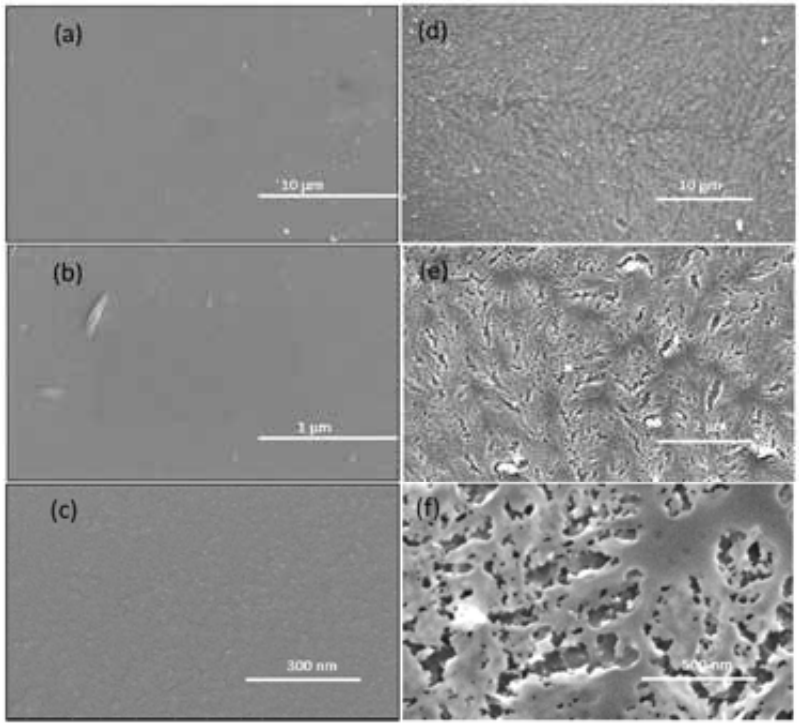

Fig. 6: SEM images for Al_2O_3 for NP-based ink (a–c), and mixed precursors NP (d–f).

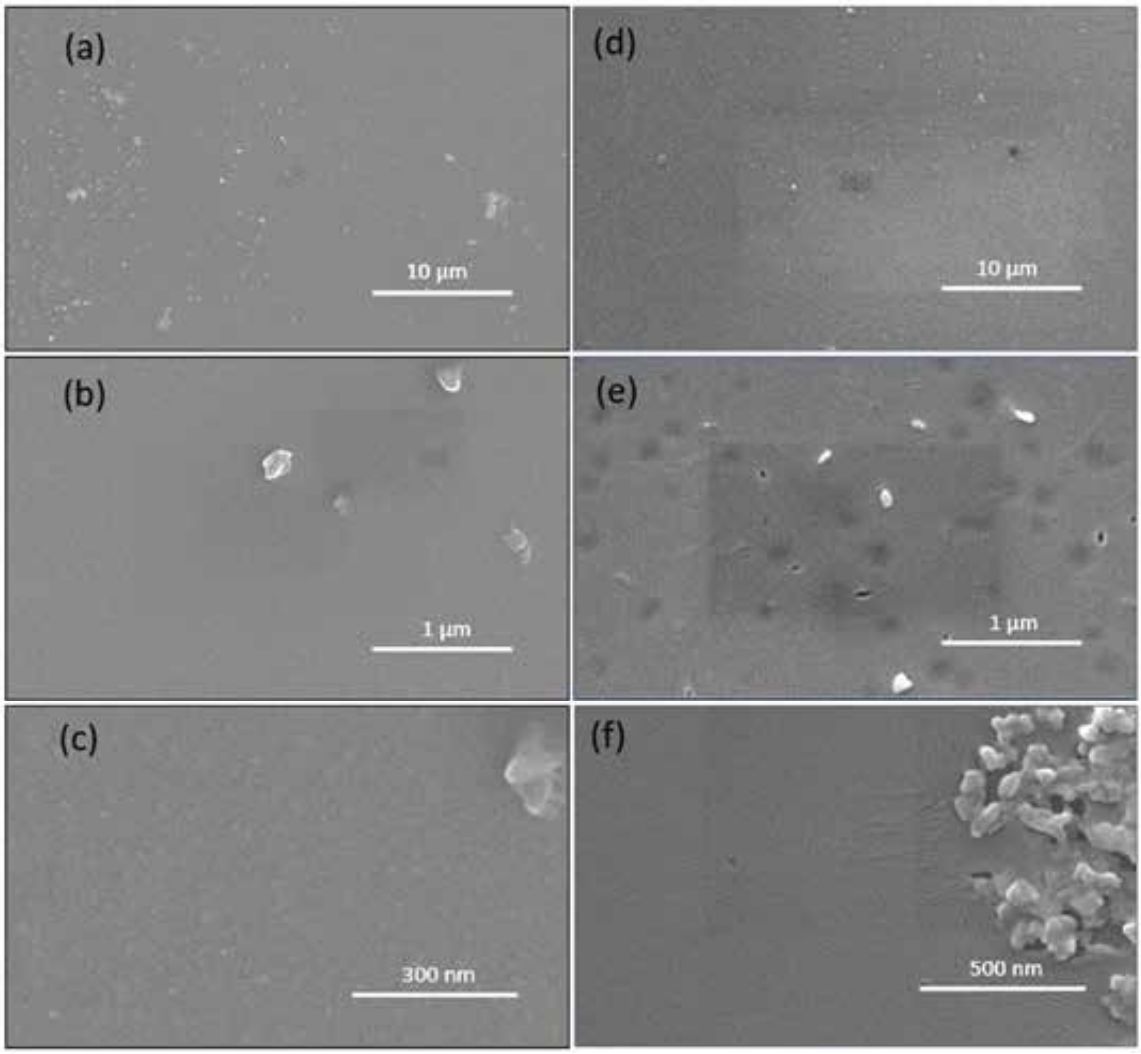

Fig. 7: SEM images for TiO_2 for NP-based ink (a–c), and mixed precursors NP (d–f).

samples (Fig. 4 to 7 c and f). Particle density and surface roughness were significant in such samples. In general, the NP sizes were uniform and spherical in ZnO and SnO_2 mixed precursors. They were dense, uniformly distributed, and well-connected over the surface. Similar to the results of Firooz *et al.,* (2008) and Lu *et al.,* (2010), a spherical morphology with porous, regular, foam-like structure particles was observed in both precursors. The synthesis procedure used in preparing SnO_2 mixed ink was similar to that used by Firooz *et al.,* (2008) to produce SnO_2 NP. They used $SnCl_2{\cdot}2H_2O$ as a precursor, whereas $SnCl_2{\cdot}2H_2O$ and SnO_2 NP were used in the present work. In both cases, SnO_2 NP were formed. In the case of ZnO, the NP were similar to the one produced by Lu *et al.,* (2010). They used zinc acetate as a primary precursor and deposited it using spin-coating techniques. According to Firooz *et al.,* (2008), the material's morphology was affected by the type of precursor and surfactant used to prepare the precursor. Parallelogram features were found in the SEM figure of the ZnO mixed thin film (Fig. 4 (d) and (e)) and a flower-like shape in the SnO_2 mixed thin film (Fig. 5e). On the contrary, the Al_2O_3 mixed thin film showed a leaf-like structure, and the TiO_2 mixed thin film exhibited an agglomeration of particles in some areas rather than a homogeneous

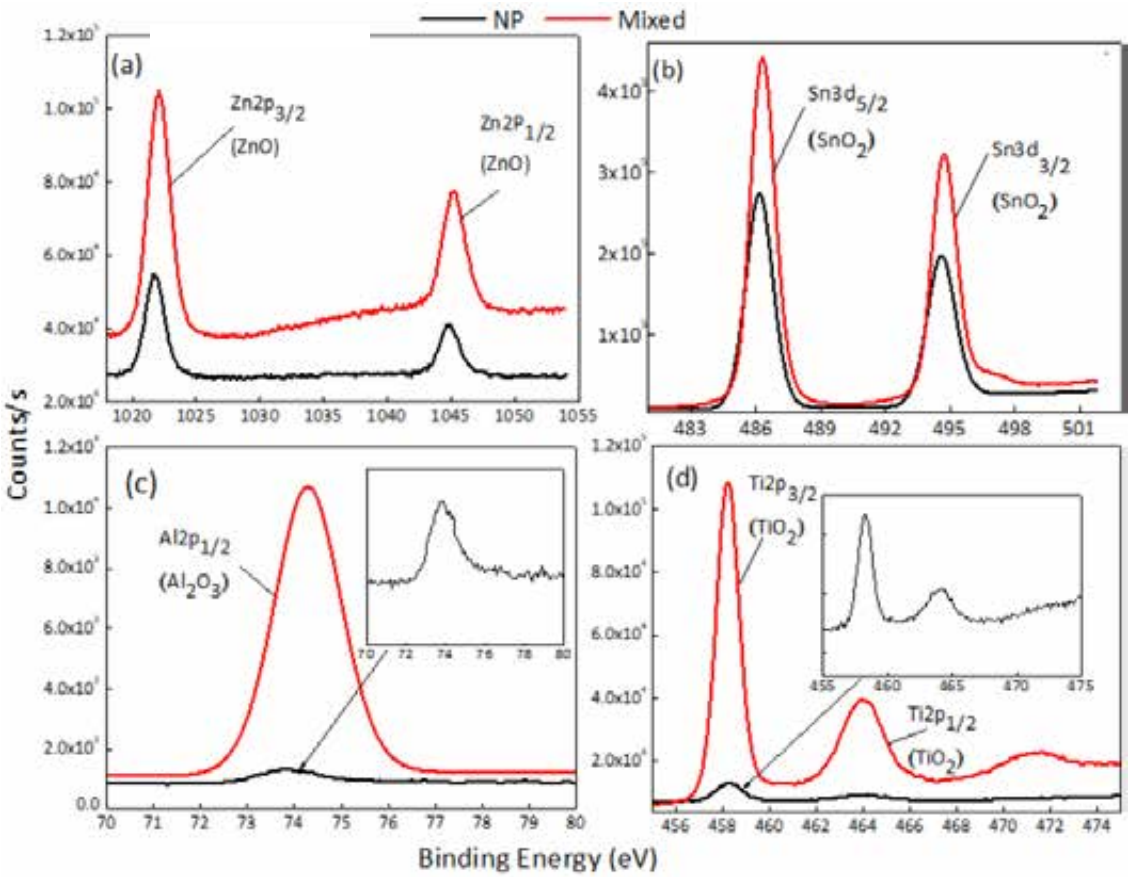

Fig. 8: XPS results of NP, salt, and mixed-based inks: (a) ZnO, (b) SnO_2, (c) Al_2O_3, and (d) TiO_2.

coverage to the substrate (see Fig. 6e and Fig. 7f). In TiO_2 mixed thin films, the granular structure can be seen in some surface areas. This may negatively affect mechanical stability, as these agglomerations adhere to the surface by the weak Van der Waals forces (Shang *et al.,* 2016). The stability over time of these coatings should be further investigated. In the case of TiO_2, the coatings exhibit a similar structure as that observed by Legrand-Buscema *et al.,* (2002), in which the samples were annealed at 400°C. The grain size was claimed to be smaller, and the porosity was lower with a low annealing temperature (<500°C). These results are in good agreement with those reported by Saini *et al.,* (2007).

Chemical properties

Fig. 8 shows the XPS results with the Zn2p spectra representing the binding energies of $Zn2p_{1/2}$ and $Zn2p_{3/2}$ for Zn^{2+}-related peaks located at 1044.7 and 1021.5 eV, respectively (Chiu *et al.,* 2015). Similarly, the Al_2O_3 sample demonstrated that the Al2p spectra were decomposed into two peaks at a binding energy of 74.5 eV for the $Al2p_{1/2}$, corresponding to the peak Al–O (Bouabibsa *et al.,* 2018). For TiO_2, the Ti2p had two spin-orbital splittings of $Ti2p_{3/2}$ at 458.5 eV and $Ti2p_{1/2}$ at 464.3 eV. These positions indicated a Ti^{4+} valence state of TiO_2 (Potlog *et al.,* 2014). However, the Sn3d core-level spectrum showed spin-orbital splittings of $Sn3d_{5/2}$ and $Sn3d_{3/2}$. The binding energy position of the $Sn3d_{5/2}$ component was located at 486.0eV, while the binding energy position of the $Sn3d_{3/2}$ component was located at 495.0 eV, corresponding to a SnO_2 state (Xia *et al.,* 2014). No clear signal from the metallic Sn at 485.0eV can be observed. The corresponding O1s spectrum in all samples was also given. The fitting indicated a metal–O component at 530 eV and other carbon-related contamination at higher binding energies (Lortie *et al.,* 2015).

Anti-soiling properties

Contact angle measurements

The CA measurement was higher in NP coatings than in the mixed ones, and this was found in all the tested samples, except for ZnO, where the CA was approximately 33° in NP coatings. The smallest CA among all samples was 8.5° in Al_2O_3 mixed coating, while the highest was 47.8° in TiO_2 mixed coating. Similar results were obtained by a previous work on TiO_2 nanofilms developed for anti-soiling application, which reported a CA of approximately 41° (Buffiere *et al.,* 2020). Therefore, all coated layers tended to be hydrophilic/super-hydrophilic. SnO_2 showed the lowest CA in general. Paul *et al.,* (2014) reported a CA of 11.8°, which was close to the values obtained in the present study, whereas the CA of TiO_2 was slightly higher, with a value of 37.4 ° (Talinungsang *et al.,* 2017). The presence of fine NP in both thin film types of SnO_2 samples increased the surface roughness, leading to a relatively low CA and thus enhanced wettability and hydrophilicity properties. They have a super-hydrophilic nature with a CA close to 0°. In this study, the CA of ZnO was lower than that reported by Jongnavakit *et al.,* (2012), considering the same annealing temperature. Jongnavakit *et al.,* (2012) reported that the lowest CA was 58° for the

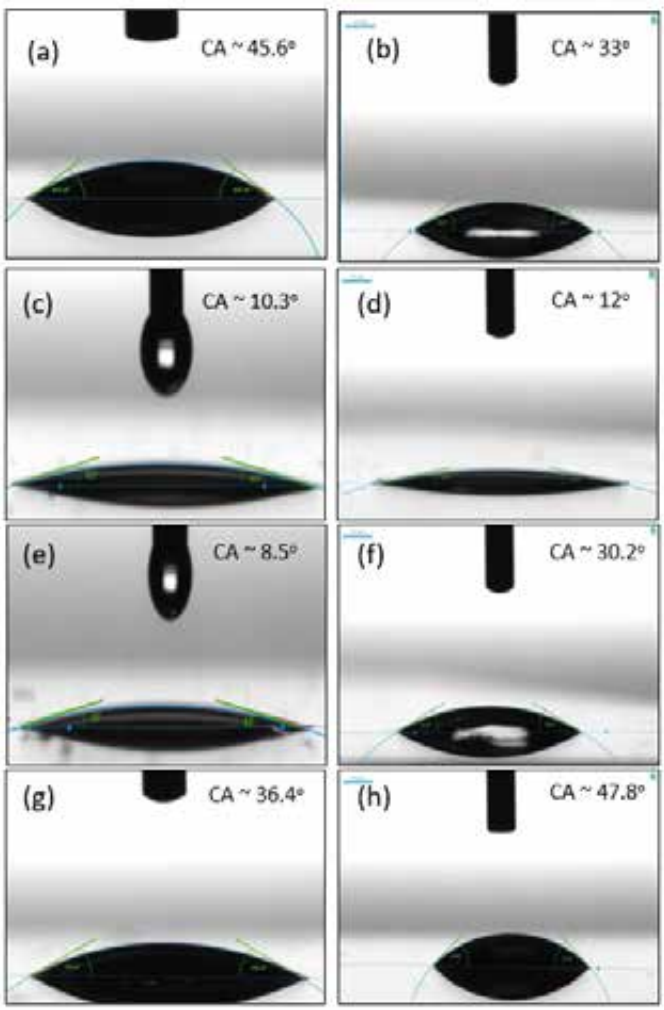

Fig. 9: Contact angle measurements to assess the hydrophilicity of (a, b) ZnO-coated samples based on mixed ink and NP ink; (c, d) SnO_2-coated samples based on mixed ink and NP ink; (e, f) Al_2O_3-coated samples based on mixed ink and NP ink; (g, h) TiO_2-coated samples based on mixed ink and NP ink.

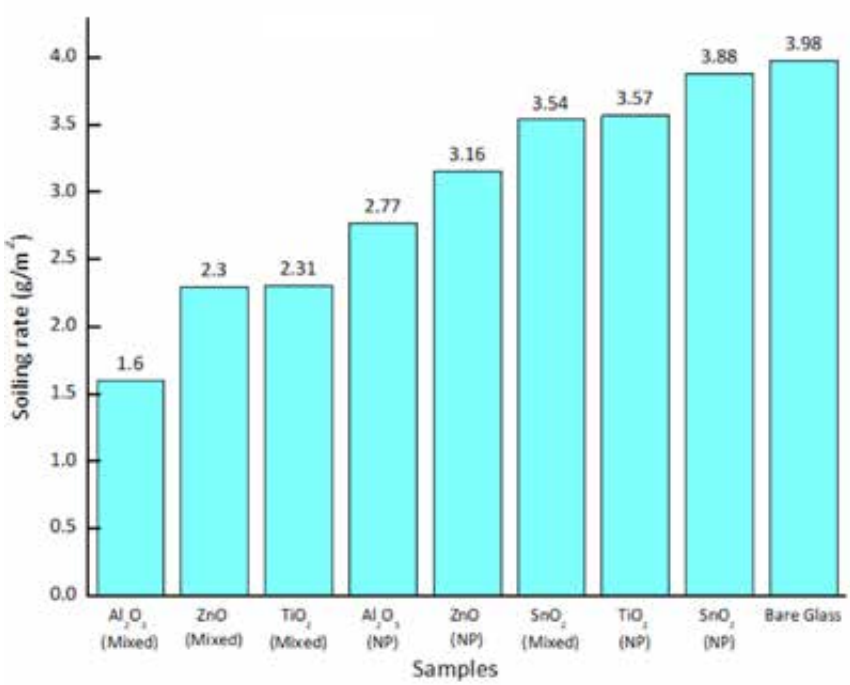

Fig. 10: Dust deposition rate for 22 days on uncoated versus coated samples.

sample prepared by dip-coating with a withdrawal speed of 3 centimeters per minute (cm/min) (Na *et al.,* 2019), whereas Lin *et al.,* (2009) reported a CA of approximately 60°. However, the CA was comparable with that reported by Lu *et al.,* (2010), when exposed to UV light for 10 min. According to Wang *et al.,* (2004), the CA of Al_2O_3 was 5°, which was in agreement with the CA of 8.5° of the mixed-based thin film in the present study. On the contrary, the CA of the NP-based thin film was similar to the results obtained by Na *et al.,* (2019) where the Al_2O_3 films were printed using a screen mask. However, Cho *et al.,* (2018) deposited Al_2O_3 NP by spray techniques. Their CA was 62°, which was significantly higher than the CA value of the NP-based thin film measured in the present study. Accordingly, the surface's hydrophilicity might be enhanced using different precursors (Fig. 9) and is dependent on the deposition techniques, as the morphology and roughness of the coated layer were affected and, accordingly, the CA values were affected. Finally, the hydrophilic property is critical in reducing the frequency of mechanical cleaning, especially in arid regions, as it reduces and releases the burden on water use, which is a scarce resource in such regions (Isaifan *et al.,* 2018).

Outdoor experiment

To accurately assess the process of dust accumulation on surfaces over time and decouple the influence of other factors such as the tilt angle, samples were placed horizontally, and the dust deposition rate is plotted in Fig. 10. Weather conditions were reported during the study period. The temperature ranged from 14°C to 40°C, the humidity was 49% on average, and the wind speed was 3.88 meters per second (m/s) on average. According to Gholami *et al.,* (2017), the results might not be applicable for the same location in other weather conditions; however, they gave a deep insight into the soiling–substrate relation. For all films, dust accumulation on the surface increased with exposure time. However, as shown in Fig. 10, which shows the dust deposition rate per surface area, a significant decrease was found in the dust deposition rate (between 2.51% and 59.80% reductions) on all coated samples compared with the bare glass substrate. All mixed thin films, except for SnO_2, showed the minimum dust deposition rates. Al_2O_3 mixed-based ink sample showed the lowest value, while the SnO_2 NP-based ink sample showed the highest one. Therefore, the mixed-based inks, especially Al_2O_3, ZnO, and TiO_2,

are promising materials for ASC applications. This is because the salt-based ink lowers the surface energy (i.e., enhances hydrophilicity), whereas the NP-based ink boosts the surface roughness, which enhances the anti-soiling properties (Quan *et al.,* 2017). Furthermore, nano-voids and surface roughness enhance the transmittance and reduce the reflection (Kauppinen *et al.,* 2017). NP-based ink comes as another alternative in which Al_2O_3, ZnO, and TiO_2 have proven to be efficient ASCs. Furthermore, for both ink types (NP and mixed-based inks), Al_2O_3 coating showed the best anti-soiling performance, whereas SnO_2 demonstrated the lowest one.

CONCLUSIONS

Soiling is one of the main issues inherent to PV applications for energy generation, especially in desert regions where the weather is characterized by high levels of particulate matter and dust formation. Although several cleaning methods have been suggested, the ASC is one of the promising mitigation techniques for dust accumulation. It reduces the operational and maintenance costs and associated cleaning water consumption. This study investigated the deposition of metal oxide thin films prepared by inkjet printing. To the best of the authors' knowledge, this is the first study to report on using films developed through inkjet printing for anti-soiling applications. The fabricated films were extensively characterized and have different textures and morphologies. Two metal oxide precursors were tested, namely, the NP ink and the mixed-based ink. The coated thin films degraded the substrate's transmittance for nearly all precursors; however, a better optical performance was observed with the NP-based coatings. This enhanced performance might be due to a lower reflection triggered by the NP's voids, which reduce the spectra scattering and deterioration and, accordingly, boost the optical transmittance. The surface morphology and profile of the coated layers were also evaluated. NPs were much more visible in mixed-based coatings than in NP-based ones. The CA values ranged from super-hydrophilic to hydrophilic (minimum of 8.5° and maximum of 47.8°). To validate the results of the outdoor tests, anti-soiling properties were further tested by exposing the samples in one of the open-air sites of Qatar University. The outdoor experiment revealed that mixed-based thin films were better in reducing dust deposition than NP-based thin films and bare glass. More specifically, approximately 60% less dust was deposited on the best-performing film (Al_2O_3 mixed-based ink) compared with bare glass. Furthermore, Al_2O_3, ZnO, and TiO_2 are promising materials for ASC applications for both ink types. Further studies on the efficiency, mechanical stability, and coating properties of anti-soiling films should be performed, especially in the outdoor environment. Moreover, measuring the effect of radiation and power output with and without coatings is recommended for practical applications and commercialization purposes.

AUTHOR CONTRIBUTIONS

E. Fares performed the experimental work, conducted the literature review, and prepared the manuscript.

B. Aissa analyzed and interpreted the film characterization data. R.J. Isaifan analyzed and interpreted the application and outdoor experimental results data, and finalized the article.

ACKNOWLEDGMENT

The authors acknowledge the support provided by Hamad Bin Khalifa University, Qatar Foundation, and Qatar University.

CONFLICT OF INTEREST

The authors declare no potential conflict of interest regarding the publication of this work. In addition, the ethical issues including plagiarism, informed consent, misconduct, data fabrication and, or falsification, double publication and, or submission, and redundancy have been completely witnessed by the authors.

OPEN ACCESS

PUBLISHER'S NOTE

GJESM Publisher remains neutral with regard to jurisdictional claims in published maps and institutional affiliations.

ABBREVIATIONS

%	Percent
A (%)	absorbance (%)
$Al(NO_3)_3\ 9H_2O$	aluminum nitrate hydrate
Al_2O_3	aluminum oxide
ASC	anti-soiling coating
°C	degree Celsius
CA	contact angle
cm/min	centimeters per minute
DMP	Dimatix Materials Printer
EG	ethylene glycol
eV	electronvolt
g	Gram
GI-XRD	grazing incidence X-ray diffraction
IPA	isopropanol
kV	kilovolts
mA	milliamperes
MgF_2	magnesium fluoride
Min	minutes
µL	microliters
mL	milliliters
µm	micrometer
mm	millimeters
mN/m	millinewton per meter
mPa.s	millipascal second
m/s	meters per second
nm	nanometer
NP	nanoparticles
pL	picoliter
PV	photovoltaic
SEM	scanning electron microscopy
SiO_2	silicon dioxide
SnO_2	tin dioxide
$SnCl_2{\cdot}2H_2O$	tin chloride hydrate
R (%)	reflection (%)
T (%)	transmittance (%)
TAA	titanium diisopropoxide bis(acetylacetonate)
TiO_2	titanium dioxide
TiO_2/SiO_2	titanium and silicon dioxides
UV	ultraviolet
UV-Vis	ultraviolet-visible
V	volt
WO_3	tungsten trioxide
XPS	X-ray photoelectron spectrometer
XRD	X-ray powder diffraction
$Zn(NO_3)_2.6H_2O$	zinc nitrates
ZnO	zinc oxide

REFERENCES

Alnaser, N.W.; Al Othman, M.J.; Dakhel, A.A.; Batarseh, I.; Lee, J.K.; Najmaii, S.; Alothman A.; Al Shawaikh H.; Alnaser W.E., (2018). Comparison between the performance of man-made and naturally cleaned PV panels in a middle of a desert. Renew. Sustain. Energy Rev., 82: 1048–1055 **(8 Pages).**

Arabatzis, I.; Todorova, N.; Fasaki, I.; Tsesmeli, C.; Peppas, A.; Li, W.X.; Zhao, Z., (2018). Photocatalytic, self-cleaning, anti-reflective coating for photovoltaic panels: Characterization and monitoring in real conditions. Sol. Energy., 159: 251–259 **(9 Pages).**

Aziz, M.; Saber Abbas, S.; Wan Baharom, W.R., (2013). Size-controlled synthesis of SnO_2 nanoparticles by sol-gel method. Mater. Lett., 91: 31–34 **(4 Pages).**

Bahattab, M.A.; Alhomoudi, I. A.; Alhussaini, M.I.; Mirza, M.; Hegmann, J.; Glaubitt, W.; Löbmann, P., (2016). Anti-soiling surfaces for PV applications prepared by sol-gel processing: Comparison of laboratory testing and outdoor exposure. Sol. Energy Mater. Sol. Cells. 157: 422–428 **(7 Pages).**

Bouabibsa, I.; Lamri, S.; Sanchette, F., (2018). Structure, mechanical and tribological properties of Me-doped diamond-like carbon (DLC) (Me = Al, Ti, or Nb) hydrogenated amorphous carbon coatings. Coatings. 8 (10): **(15 Pages).**

Buffiere, M.; Ali, K.; Fares, E.; Samara, A.; Shetty, A.R.; Al Hassan, O.; Belaidi, A., (2020). Inkjet-printed compact TiO2 electron transport layer for perovskite solar cells. Energy Technol., 8 (10): 2000330 (7 **Pages).**

Bukhari, S.F.; Lisco, F.; Moghim, T.B.; Taylor, A.; Walls, J.M., (2019). Development of a hydrophobic, anti-soiling coating for PV module cover glass. In 2019 IEEE 46th Photovoltaic Specialists Conference (PVSC). 15-21 June. Chicago, USA, 2849-2853 **(5 Pages).**

Chiu, F.C.; Chiang, W.P., (2015). Trap exploration in amorphous boron-doped ZnO films. Materials. 8(9): 5795–5805 **(11 Pages)**.

Cho, M.Y.; Park, S.J.; Kim, S.M.; Lee, D.W.; Kim, H.K.; Koo, S.M.; Moon, K.S; Oh J.M., (2018). Hydrophobicity and transparency of Al2O3-based poly-tetra-fluoro-ethylene composite thin films using aerosol deposition. Ceram. Int., 44 (14): 16548–16555 **(8 Pages).**

Cummins, G.; Desmulliez, M.P.Y., (2012). Inkjet printing of conductive materials: A review. Circuit World, 38 (4): 193–213 **(21 Pages)**.

Eihorn, A.; Micheli, L.; Miller, D.C.; Simpson, L.J.; Moutinho, H.R.; To, B.; Lanaghan, C.L.; Muller, M.T.; Toth, S.; John, J.J.; Warade, S.; Kottantharayil, A.; Engtrakul, C., (2019). Evaluation of soiling and potential mitigation approaches on photovoltaic glass. IEEE J. Photovoltaics, 9 (1): 233–239 **(7 Pages).**

Firooz, A.A.; Mahjoub, A.R.; Khodadadi, A. A., (2008). Preparation of SnO2 nanoparticles and nanorods by using a hydrothermal method at low temperature. Mater. Lett., 62 (12–13): 1789–1792 **(4 Pages)**.

Gholami, A.; Alemrajabi, A.A.; Saboonchi, A., (2017). Experimental study of self-cleaning property of titanium dioxide and nanospray coatings in solar applications. Sol. Energy., 157: 559–565 **(7 Pages).**

Huang, Y.; Lin, J.; Du, H.; Gao, L.; Yan, H., (2006). Preparation and photoluminescence properties of ZnO/amorphous-BaTiO3 thin-films by sol–gel process. Mater. Lett., 60 (29):3818-3821 **(4 Pages).**

Ilse, K.K.; Figgis, B.W.; Werner, M.; Naumann, V.; Hagendorf, C.; Pöllmann, H.; Bagdahn, J., (2018). Comprehensive analysis of soiling and cementation processes on PV modules in Qatar. Sol. Energy Mater. Sol. Cells, 186 (2018): 309–323 **(15 Pages).**

Isaifan, R.J.; Johnson, D.; Mansour, S.; Samara, A.; Suwaileh, W.; Kakosimos, K., (2018). Theoretical and experimental characterization of efficient anti-dust coatings under desert conditions. J. Thin Film. Res., 2 (1): 25–29 **(5 Pages).**

Isaifan, R.J.; Samara, A.; Suwaileh, W.; Johnson, D.; Yiming, W.; Abdallah, A.A.; Aïssa, B., (2017). Improved self-cleaning properties of an efficient and easy to scale up Tio2 thin films prepared by adsorptive self-assembly. Sci. Rep., 7 (1): 1-9 **(9 Pages).**

Hossain, M.I.; Aïssa, B.; Samara, A.; Mansour, S.A.; Broussillou, C.A.; Bermudez Benito, V., (2021). Hydrophilic antireflection and antidust silica coatings. ACS Omega., 6(8): 5276-5286 **(11 Pages).**

Javed, W.; Wubulikasimu, Y.; Figgis, B.; Guo, B., (2017). Characterization of dust accumulated on photovoltaic panels in Doha, Qatar. Sol. Energy., 142: 123–135 **(13 Pages).**

Jesus, M.A.M. L. de; Timò, G.; Agustín-Sáenz, C.; Braceras, I.; Cornelli, M.; Ferreira, A.de M., (2018). Anti-soiling coatings for solar cell cover glass: Climate and surface properties influence. Sol. Energy Mater. Sol. Cells, 185 (2018): 517–523 **(7 Pages).**

Jongnavakit, P.; Amornpitoksuk, P.; Suwanboon, S.; Ratana, T., (2012). Surface and photocatalytic properties of ZnO thin film prepared by sol-gel method. Thin Solid Films, 520 (17): 5561–5567 **(7 Pages).**

Karabay, I.; Aydin Yüksel, S.; Ongül, F.; Öztürk, S.; Asli, M., (2012). Structural and optical characterization of TiO2 thin films prepared by sol-gel process. In Acta Phys. Pol., 121: 265-267 **(3 Pages).**

Kareem, K.S.A.; Rao, K.N.; Phani, A.R.; Rani, R.U.; Sharma, A.K., (2011). Optical and structural properties of nanostructured oxide thin films by sol-gel technique. In The American Institute of Physics Conference Proceedings. 23-25 May. Kerala, India, 1391: 600–602 **(3 Pages).**

Kauppinen, C.; Isakov, K.; Sopanen, M., (2017). Grass-like alumina with low refractive index for scalable, broadband, omnidirectional anti-reflection coatings on glass using atomic layer deposition. ACS Appl. Mater. Interfaces, 9 (17): 15038–15043 **(6 Pages).**

Lee, H.; Yi, A.; Choi, J.; Ko, D.-H.; Kim, H., (2022). Texturing of polydimethylsiloxane surface for anti-reflective films with super-hydrophobicity in solar cell application. Appl. Surf. Sci., 584: 152625 **(8 pages).**

Legrand-Buscema, C.; Malibert, C.; Bach, S., (2002). Elaboration and characterization of thin films of TiO2 prepared by sol-gel process. Thin Solid Films, 418 (2): 79–84 **(6 Pages).**

Li, X.; He, J.; Liu, W., (2013). Broadband anti-reflective and water-repellent coatings on glass substrates for self-cleaning photovoltaic cells. Mater. Res. Bull., 48 (7): 2522–2528 **(7 Pages).**

Lin, L.Y.; Kim, D.E., (2009). Effect of annealing temperature on the tribological behavior of ZnO films prepared by sol-gel method. Thin Solid Films, 517 (5): 1690–1700 **(11 Pages).**

Liu, X.; Tarn, T.J.; Huang, F.; Fan, J., (2015). Recent advances in inkjet printing synthesis of functional metal oxides. Particuology, 19 (2015): 1–13 **(14 Pages).**

Lortie, M.; Isaifan, R.J.; Liu, Y.; Mommers, S., (2015). Synthesis of CuNi/C and CuNi/-Al2O3 catalysts for the reverse water gas shift reaction. Int. J. Chem. Eng., 2015: 750689 **(9 pages).**

Lu, J.; Huang, K.; Chen, X.; Zhu, J.; Meng, F.; Song, X.; Sun, Z., (2010). Reversible wettability of nanostructured ZnO thin films by sol-gel method. Appl. Surf. Sci., 256 (14): 4720–4723 **(4 Pages).**

Micheli, L.; Muller, M., (2017). Seasonal trends of soiling on PV

systems. 2017 IEEE 44th Photovoltaic Conference (PVSC). 25-30 June. Washington, USA, 2301-2306 **(8 Pages).**

Na, M.J.; Yang, H.; Jung, H.J.; Park, S.D., (2019). Robust hydrophobic surface driven by Al2O3/glass composite coatings. Surf. Coatings Technol., 372(2019): 134–139 **(6 Pages).**

Nunes, D.; Pimentel, A.; Santos, L.; Barquinha, P.; Pereira, L.; Fortunato, E.; Martins, R., (2019). Oxide materials for energy applications. Met. Oxide Nanostructures. **(36 Pages).**

Oh, W.; Kang, B.; Choi, S.; Bae, S.; Jeong, S.; Kim, S.M.; Lee, H.S.; Kim, D.; Hwang, H.; Chan, Sung. I., (2016). Evaluation of anti-soiling and anti-reflection coating for photovoltaic modules. J. Nanosci. Nanotechnol., 16 (10): 10689–10692 **(4 Pages).**

Ota, Y.; Ahmad, N.; Nishioka, K., (2016). A 3.2% output increase in an existing photovoltaic system using an anti-reflection and anti-soiling silica-based coat. Sol. Energy., 136: 547–552 **(6 Pages).**

Paul S.; Hossain M.F.; Islam M.H.; Raihan M.A.; Chakladar S., (2014). Optical properties of ZnO thin films prepared by automatic sol-gel method. In 2013 IEEE International conference on Electrical Information and Communication Technology (EICT). 13-15 February. Khulna, Bangladesh, 1-4 **(6 Pages).**

Pendse, S.; Chandra, S.R., K.; Narendra, C.; Murugan, K.; Sakthivel, S., (2018). Dual-functional broadband anti-reflective and hydrophobic films for solar and optical applications. Sol. Energy., 163 (2018): 425–433 **(9 Pages).**

Perez-Tomas, A.; Mingorance, A.; Tanenbaum, D.; Lira-Cantú, M., (2018). Metal oxides in photovoltaics: All-oxide, ferroic, and perovskite solar cells. Metal oxides, the future of semiconductor oxides in Next-generation solar cells. 267–356. Elsevier **(90 Pages).**

Pescheux, A.C.; Raccurt, O.; Bourdon, D.; Le Baron, E., (2020). Accelerated aging tests and characterizations of innovated anti-soiling coatings for solar receiver glasses. Mater. Chem. Phys., 256: 123646 **(8 Pages).**

Piliougine, M.; Cañete, C.; Moreno, R.; Carretero, J.; Hirose, J.; Ogawa, S.; Sidrach-de-Cardona, M., (2013). Comparative analysis of energy produced by photovoltaic modules with anti-soiling coated surface in arid climates. Appl. Energy, 112(C): 626–634 **(9 Pages).**

Polizos, G.; Jang, G.G.; Smith, D.B.; List, F.A.; Lassiter, M.G.; Park, J.; Datskos, P.G., (2018a). Transparent superhydrophobic surfaces using a spray coating process. Sol. Energy Mater. Sol. Cells, 176: 405–410 **(6 Pages).**

Polizos, G.; Sharma, J.K.; Smith, D.B.; Tuncer, E.; Park, J.; Voylov, D.; Sokolov, A.P.; Meyer III, H.M.; Aman, M., (2018b). Anti-soiling and highly transparent coatings with multi-scale features. Sol. Energy Mater. Sol. Cells, 188 (2018): 255–262 **(8 Pages).**

Potlog, T.; Dumitriu, P.; Dobromir, M.; Luca, D., (2014). XRD and XPS analysis of TiO2 thin films annealed in different environments. J. Mater. Sci. Eng. B, 4 (6): **(8 Pages).**

Quan, Y.Y.; Zhang, L.Z., (2017). Experimental investigation of the anti-dust effect of transparent hydrophobic coatings applied for solar cell covering glass. Sol. Energy Mater. Sol. Cells, 160: 382–389 **(8 Pages).**

Rieu, M.; Camara, M.; Tournier, G.; Viricelle, J.-P.; Pijolat, C.; de Rooij, N.F.; Briand, D., (2016). Fully inkjet printed SnO2 gas sensor on plastic substrate. Sensors Actuators B Chem., 236: 1091–1097 **(7 Pages).**

Said, S.A.; Al-Aqeeli, N.; Walwil, H.M., (2015). The potential of using textured and anti-reflective coated glasses in minimizing dust fouling. Sol. Energy, 113: 295–302 **(8 Pages).**

Saini, K.K.; Sharma, S.D.; Chanderkant; Kar, M.; Singh, D.; Sharma, C.P., (2007). Structural and optical properties of TiO2 thin films derived by sol-gel dip coating process. J. Non. Cryst. Solids. 353 (24–25): 2469–2473 **(5 Pages).**

Shang, Q.; Zhou, Y., (2016). Fabrication of transparent superhydrophobic porous silica coating for self-cleaning and anti-fogging. Ceram. Int., 42 (7): 8706–8712 **(7 Pages).**

Sobczyk-Guzenda, A.; Pietrzyk, B.; Szymanowski, H.; Gazicki-Lipman, M.; Jakubowski, W., (2013). Photocatalytic activity of thin TiO2 films deposited using sol-gel and plasma enhanced chemical vapor deposition methods. Ceram. Int., 39 (3): 2787–2794 **(8 Pages).**

Sueto, T.; Ota, Y.; Nishioka, K., (2013). Suppression of dust adhesion on a concentrator photovoltaic module using an anti-soiling photocatalytic coating. Sol. Energy., 97: 414–417 **(4 Pages).**

Talinungsang, N.P.; Purkayastha, D.D., (2017). SnO2/TiO2 bilayer thin films exhibiting superhydrophilic properties. In The American Institute of Physics Conference Proceedings. 26-30 December. Odisha, India, 1832: 080035 **(4 Pages).**

Thongsuwan, W.; Sroila, W.; Kumpika, T.; Kantarak, E.; Singjai, P. (2022) et al. Antireflective, photocatalytic, and superhydrophilic coating prepared by facile sparking process for photovoltaic panels. Sci. Rep., 12: 1675 **(15 pages).**

Wang, J.; Yang, S.; Chen, M.; Xue, Q., (2004). Preparation and characterization of arachidic acid self-assembled monolayers on glass substrate coated with sol-gel Al2O3 thin film. Surf. Coatings Technol., 176 (2): 229–235 **(7 Pages).**

Wang, Y.; Li, B.; Liu, T.; Xu, C.; Ge, Z., (2014). Controllable fabrication of superhydrophobic TiO2 coating with improved transparency and thermostability. Colloids Surf., A 441: 298–305 **(8 Pages).**

Xia, W.; Wang, H.; Zeng, X.; Han, J.; Zhu, J.; Zhou, M.; Wu, S., (2014). High-efficiency photocatalytic activity of type II SnO/Sn3O4 heterostructures via interfacial charge transfer. Cryst. Eng. Comm., 16 (30): 6841–6847 **(7 Pages).**

Yamaguchi, N.; Tadanaga, K.; Matsuda, A.; Minami, T.; Tatsumisago, M., (2005). Anti-reflective coatings of flower-like alumina on various glass substrates by the sol-gel process with the hot water treatment. J. Sol-Gel Sci. Technol., 33 (1): 117–120 **(4 Pages).**

AUTHOR (S) BIOSKETCHES

Fares, E., Ph.D. Candidate, College of Science and Engineering, Hamad Bin Khalifa University Qatar Foundation, Doha, Qatar.

- Email: *efares@hbku.edu.qa*
- Web of Science Researcher ID: NA
- Scopus Author ID: NA
- ORCID: 0000-0001-5989-2590
- Homepage: http://www.qu.edu.qa/engineering/Academic-Departments/Department-of-Mechanical-and-Industrial-Engineering/Faculty-and-Staff

Aissa, B. Ph.D., Assistant Professor, Qatar Environment and Energy Research Institute, Hamad Bin Khalifa University, Qatar Founda-tion, Doha, Qatar

- Email: *baissa@hbku.edu.qa*
- Web of Science Researcher ID: I-4522-2014
- Scopus Author ID: NA
- ORCID: 0000-0002-4768-9891
- Homepage: https://www.hbku.edu.qa/en/staff/brahim-aissa

Isaifan, R., Ph.D., Joint Faculty, College of Science and Engineering, Hamad Bin Khalifa University, Qatar Foundation, Doha, Qatar.

- Email: *risaifan@hbku.edu.qa*
- Web of Science Researcher ID: AAL-9634-2020
- Scopus Author ID: 54897983000
- ORCID: 0000-0002-9590-4939
- Homepage: https://www.hbku.edu.qa/ar/staff/rima-jamal-isaifan

HOW TO CITE THIS ARTICLE

Fares, E.; Aïssa, B.; Isaifan,R.J. (2022). Inkjet printing of metal oxide coatings for enhanced photovoltaic soiling environmental applications. Global J. Environ. Sci.Manage., 8(4): 485-502.

DOI: 10.22034/gjesm.2022.04.03

url: https://www.gjesm.net/article_250777.html